Polish Society of Composite Materials
Polskie Towarzystwo Materiałów Kompozytowych

22: 2 (2022) 72-78

COMPOSITES THEORY AND PRACTICE
ISSN: 2084-6096
ISSN (online): 2299-128X

**Cantekin Kaykılarlı[1,2]*, Zehra Altınışık[1], E. Can Kılıç[3], Deniz Uzunsoy[2], H. Aygül Yeprem[1]**

*[1] Yıldız Technical University, Metallurgy and Materials Engineering Department, 34210, Istanbul, Turkey*
*[2] Bursa Technical University, Metallurgy and Materials Engineering Department, 16310, Yıldırım, Turkey*
*[3] Yıldız Technical University, Chemical Engineering Department, 34210, Istanbul, Turkey*
**Corresponding author. E-mail: cantekin.kaykilarli@btu.edu.tr*

*Received (Otrzymano) 24.01.2022*

# ALUMINIUM OXIDE ($Al_2O_3$)-FEW LAYER GRAPHENE (FLG) REINFORCED ALUMINIUM HYBRID COMPOSITES

**The present study investigates the microstructural and mechanical properties of few layer graphene (FLG, 0.1 to 5 wt.%) and aluminium oxide ($Al_2O_3$, 4 to 20 wt.%) reinforced Al6061 matrix composites prepared via mechanical alloying (MA), uniaxial pressing and pressureless sintering. The effects of the amounts of $Al_2O_3$ and FLG were studied. MA was carried out at 300 rpm for 3 h in a planetary ball mill in argon atmosphere. The mechanically alloyed (MAed) powders were compacted via uniaxial pressing (400 MPa) and sintering (620°C, 2 h). The microstructural and mechanical properties of the Al-x$Al_2O_3$-yFLG powders and bulk samples were investigated via X-ray diffraction (XRD), light microscopy (LM), scanning electron microscopy (SEM), energy dispersive spectroscopy (EDS), the Archimedes' method and a hardness test. In the XRD analysis, the aluminium carbide ($Al_4C_3$) phase was not detected. The SEM, LM micrographs and EDS results show that the produced composites have a homogeneous structure. Based on the Archimedes' method, the densification rates of the reinforced samples were higher than the unreinforced sample. The Al-20$Al_2O_3$-3FLG sample exhibited the highest relative density, 99.25%. According to the hardness measurements, the highest hardness value was 87.28 HV for the Al-20$Al_2O_3$-1FLG composite and increased twofold compared to Al6061.**

**Keywords: Al matrix composites, Al6061, aluminium oxide, few-layer graphene, powder metallurgy, hardness**

## INTRODUCTION

Metal matrix composites (MMCs) are currently being chosen to replace conventional metallic materials in many engineering applications due to their outstanding properties. MMCs are used in the aerospace, construction, defence, electronic packaging and automotive industries. They potentially provide a higher strength-to-weight ratio, good thermal fatigue and creep resistance, and a lower thermal expansion coefficient. The properties of MMCs are affected by the particle size distribution, particle type, volume ratio and reinforcement phase. In MMCs, the reinforcement materials should be homogeneously distributed in the matrix, and their agglomeration should be prevented. Some of the most commonly used matrix materials in MMCs are Al, Mg, Ti and their alloys. Aluminium matrix composites (AMCs) stand out owing to their low density, high toughness, tensile strength and elastic modulus, excellent wear and corrosion resistance. At the same time, the mechanical properties of AMCs can be modified by heat treatment. In addition, Al alloys are characterized by good corrosion resistance and outstanding mechanical properties, but some problems still need to be solved like low wear and seizure resistance. To date, additives such as WC, $Al_2O_3$, fly ash, graphite, mica, coconut shell charcoal and SiC have been successfully incorporated in the Al matrix, helping to significantly improve the properties of the alloy [1-14].

Heat treatable Al6061 alloys containing magnesium and silicon as their major alloying elements exhibit outstanding corrosion resistance, moderate strength, and good weldability. They are used in the construction, automotive, and marine engineering fields [6, 15, 16].

$B_4C$, WC, $Al_2O_3$, ZrC, TiC, SiC, graphite, carbon nanotubes, graphene, and fly ash are also used to reinforce AMCs. Graphene has outstanding properties compared to other reinforcements. Graphene has a two-dimensional hexagonal lattice structure and has shown excellent mechanical, thermal and electrical properties such as superior fracture strength (130 GPa), high Young's modulus (1 TPa), high specific surface area (2630 $m^2g^{-1}$), excellent electrical conductivity ($10^8$ S/m) and good thermal conductivity (5000 $Wm^{-1}K^{-1}$) [4, 7, 9, 12, 17-21].

Al matrix composites reinforced with $Al_2O_3$ and graphene nanostructures have been produced by various methods in some recent studies. Şenel et al. [2] produced Al hybrid composites reinforced with $Al_2O_3$/GNPs binary particles via the powder metallurgy (PM) route and investigated their hardness and compressive strength. They found the highest hardness and ultimate

compressive strength for Al-30$Al_2O_3$-0.1 GNPs. The amount of GNPs exceeding 0.1 wt.% reduced the hardness and maximum compressive strength. Daha et al. [22] produced reduced graphene oxide (RGO), and $Al_2O_3$ reinforced Al metal matrix composites via PM. According to the wear test results, they observed that the addition of RGO increased the wear resistance more than $Al_2O_3$. Furthermore, the hardness of the composite samples reinforced with $Al_2O_3$ and RGO was higher than the samples reinforced with a single additive. However, increasing the amount of $Al_2O_3$ results in deterioration of the mechanical and tribological properties of the hybrid and single reinforced samples as a consequence of agglomeration. The optimum wear resistance and hardness results were found for the composites, including 0.3 wt.% RGO and 5 wt.% $Al_2O_3$. Omrani et al. [23] produced Al-graphite nanoplatelet and Al-graphite nanoplatelet-$Al_2O_3$ composites with various amounts of reinforcements by the PM route. The highest hardness results were obtained for the Al-1graphite nanoplatelet-2$Al_2O_3$ composites. Moreover, they observed that the wear rate and coefficient of friction (COF) were reduced by 93 and 43%, respectively. Kumar et al. [24] investigated the fatigue and wear behaviour of the Al6061-graphene (0.2, 0.4, 0.6 wt.%) composite produced by PM. They found that the Al6061-0.4 wt.% graphene samples have the highest hardness and the lowest wear loss. Pournaderi et al. [25] prepared Al6061-$Al_2O_3$ composites via in-situ powder metallurgy and investigated their wear behaviour. The highest wear resistance was obtained by the composite containing 20 vol.% $Al_2O_3$. Lemus et al. [26] produced Al6061-$Al_2O_3$ composites by PM and investigated the wear behaviour. They observed significant improvement in the wear resistance with $Al_2O_3$ reinforcement. There are few studies in the literature related to graphene and $Al_2O_3$ reinforcement in an Al6061 matrix. Boppana et al. [27] produced Al6061 matrix composites reinforced with $Al_2O_3$ (5, 10 and 15% by weight) and graphene (1% by weight) by the fluid metallurgy method and examined their mechanical performance. With the addition of graphene and $Al_2O_3$, there was a remarkable increase in hardness, tensile strength and yield strength. The highest values were attained by the sample reinforced with 1% by weight graphene and 15% by weight $Al_2O_3$. Soni et al. [28] produced hybrid nanocomposites based on Al6061 reinforced with $Al_2O_3$ (2% by weight) and graphene (0.5, 1, 1.5, 2 and 2.5 wt.%) by the ultrasonic-assisted melt mixing method. The mechanical properties increased with the addition of graphene and $Al_2O_3$. They determined that Al6061 reinforced with 1% by weight graphene and 2% by weight $Al_2O_3$ had the highest hardness, ultimate tensile and bending, and compressive strength. As a result, the current research tries to understand and investigate the effect of $Al_2O_3$ and FLG particles added to the Al6061 alloy.

In this study, simultaneous various additions of $Al_2O_3$ and FLG were used in multiple proportions compared to other literature studies. The present studies aimed to prepare Al6061-x$Al_2O_3$ (x = 0, 4, 8, 12 and 20 wt.%)-yFLG (y = 0.1, 0.25, 0.5, 1, 3, and 5 wt.%) composites by the PM route and investigate the microstructural and mechanical properties of the composites. Firstly, five different sample groups containing different amounts of $Al_2O_3$ and FLG were produced. Later, the $Al_2O_3$ was kept constant in the sample set that shows the best hardness result, and three more groups with different FLG ratios were produced. The effects of the $Al_2O_3$ and FLG reinforcements on the Al6061 alloy matrix were studied.

## MATERIALS AND METHODS

Al6061 (Nanografi, 99.5%, 43 μm), $Al_2O_3$ (Nanografi, 99.5%, 90-125 μm) and FLG (Nanografi, 99.9%, 5 nm) were used as the starting powders. Al6061 was used as the matrix material, and X-ray fluorescence (XRF, Rigaku SuperMini200) analysis was performed to determine its chemical composition. The obtained XRF results are given in Table 1.

TABLE 1. **Chemical composition of Al6061 [wt.%]**

| | Mg | Si | K | Fe | Cu | Zn | Ga | Al |
|---|---|---|---|---|---|---|---|---|
| Al6061 | 0.96 | 0.84 | 0.07 | 0.17 | 0.43 | 0.22 | 0.02 | 97.3 |

$Al_2O_3$ in amounts of 4, 8, 12 and 20 wt.% and FLG 0.1, 0.25, 0.5, 1, 3 and 5 wt.% were added to the Al 6061 matrix. The starting powders were mechanically alloyed (MAed) in a planetary ball mill (Fritsch$^{TM}$, Pulverisette 6) at 300 rpm for 3 h. A stainless steel milling vial (250 ml) and balls (Ø: 10 mm, ball to powder ratio: 8:1) were used in the mechanical alloying (MA) process. Additionally, as the process control agent (PCR), stearic acid (2 wt.%) was added to the powder mixtures to avoid cold welding of the Al particles and agglomeration.

After MA, the prepared powders were compacted by a hydraulic press (MSE$^{TM}$ MP0710) under the uniaxial pressure of 400 MPa to produce cylindrical preforms (diameter: 16 mm). Sintering was conducted at 620°C for 2 h in a ProthermTm PTF 15/50/610 tube furnace with a heating and cooling rate of 10°C/min under argon flow (1 l/min). X-ray diffraction (XRD, PANalytical X'Pert Pro) was employed to conduct phase analysis of the powders and bulk sample with CuKα radiation (40 kV, 40 mA). The density of the sintered samples was obtained by the Archimedes' method.

The number of layers and quality of FLG were investigated using Raman spectroscopy (Renishaw in Via Reflex). The Raman spectra were measured from 500 to 3000 $cm^{-1}$ with an excitation wavelength of 532 nm.

The theoretical density of the sintered Al6061-x$Al_2O_3$-xFLG composites was determined by the rule of mixtures (ROM) using the densities of Al 2.7 g/$cm^3$,

 

$Al_2O_3$ 3.9 g/cm$^3$ and FLG as 2.25 g/cm$^3$. ROM can be briefly explained as follows:

$$\rho_{th} = \rho_{FLG} \times V_{FLG} + \rho_m \times V_m \quad (1)$$

where $V_{FLG}$ is the volume fraction of FLG and $V_m$ is the volume fraction of the matrix materials. In addition, $\rho_{FLG}$ and $\rho_m$ are the density values of FLG and the matrix materials, respectively [29].

Microstructural analysis of the sintered samples was performed by a light microscope (LM, Nikon-Eclipse MA100) and a Zeiss Evo$^R$ LS 10 scanning electron microscope (SEM) equipped with energy dispersive spectroscopy (EDS). Hardness testing was performed with a Qness$^{TM}$ Q10 Hardness Tester under conditions of 5 kg load for 15 s, and the mean values and standard deviations were obtained based on at least ten measurements.

## RESULTS AND DISCUSSION

The XRD patterns of the Al6061-x$Al_2O_3$-yFLG powders are shown in Figure 1a. In the XRD patterns, only α-Al and α-$Al_2O_3$ phases were observed. FLG was not detected due to its low amount under the XRD detection limit. No new phases related to Al, $Al_2O_3$ and FLG were detected in the XRD analysis. Therefore, no chemical reactions occurred between the compounds during MA.

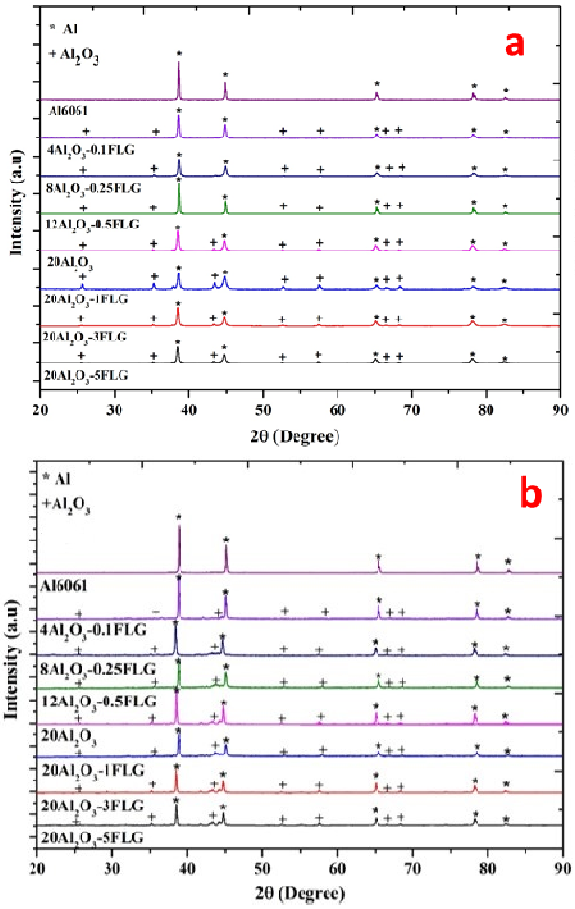


Fig. 1. XRD patterns of Al6061-x$Al_2O_3$-yFLG powders (a) and composites (b)

Especially the aluminium carbide ($Al_4C_3$) phase was not detected. The XRD patterns of the composite powders were compatible with the literature. For example, Al-Mosavi et al. produced α-$Al_2O_3$ particle reinforced AMC with various milling times. Gudlur et al. fabricated Al-$Al_2O_3$ composites at elevated temperatures via the PM route. Balaraj et al. produced micro $Al_2O_3$ particle reinforced Al6061 alloy metal composites via the liquid metallurgy technique. The XRD results obtained in the mentioned studies are compatible with our study [23, 30, 31].

The XRD patterns of the sintered Al6061-x$Al_2O_3$-yFLG composites are given in Figure 1b. According to the XRD analyses of the sintered composites, α-Al and α-$Al_2O_3$ phases were observed in all the specimens. Furthermore, the peaks related to FLG, such as C and $Al_4C_3$, were unable to be detected in the XRD analysis of the composites. Moreover, no chemical reactions between the compounds occurred during the sintering process. The XRD analyses results are consistent with previous studies. Şenel et al. produced Al-x$Al_2O_3$-yGNPs composites via the PM method. They found only α-Al and α-$Al_2O_3$ phases resulting from the XRD analysis for all the composites. Prakash et al. produced an Al6061 aluminium sheet metal reinforced with $Al_2O_3$/0.5 Gr hybrid surface nanocomposite via friction stir processing. They detected that only α-Al and α-$Al_2O_3$ phases were observed in the composites structures [2, 32, 33].

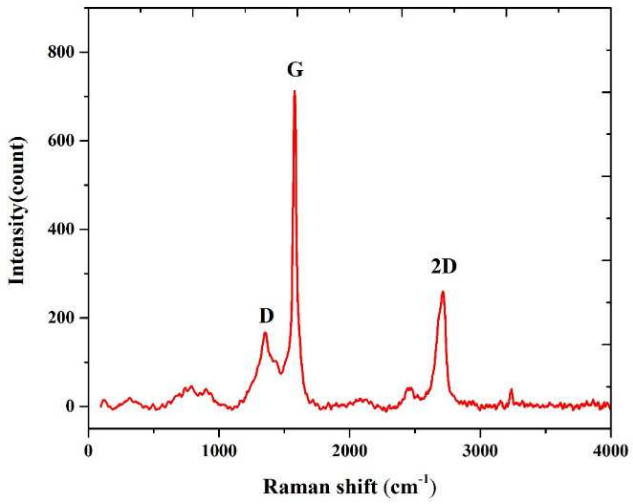


Fig. 2. Raman spectroscopy results for FLG

The Raman spectroscopy method was employed to determine the characteristic bands of FLG. The obtained Raman spectroscopy results of FLG are given in Figure 2. D, G and 2D bands are located at 1357 cm$^{-1}$, 1579 cm$^{-1}$ and 2705 cm$^{-1}$, respectively. The D band shows defects in the structure of carbon-based materials because of the lattice distortion introduced by impurities. The position and shape of the G band indicate defects, the doping effect, stress, and the number of graphene layers. The 2D band is the characteristic band of

 

graphene, and its shape is related to the number of layers [20, 34].

According to the Raman spectroscopy results, the $L_G/L_{2D}$ ratio gives information about the total graphene layers. Additionally, the $L_D/L_G$ ratio is used to detect the purity of the graphene. For graphene, the $L_D/L_G$ ratio should be between 0 and 1, and the purity of the graphene is higher when it is close to zero. In the previous literature study, for single-layer graphene the obtained $L_G/L_{2D}$ ratio was 0.25 [35]. For graphene, the detected $L_D/L_G$ and $L_G/L_{2D}$ ratios were 0.23 and 2.74, respectively. These ratios show that FLG has high purity and approximately 10 layers.

The relative density values of the sintered composites are shown in Figure 3. The relative density values of the composites vary between 90.40% and 99.25%. As seen in Figure 3, the sintered Al6061 samples had the lowest relative density (90.40%). In addition, the Al-20$Al_2O_3$-3FLG composites had the highest relative density (99.25%), nearly 10% higher than the non-reinforced Al samples. It is clearly seen that the reinforcement increased the densification rates of the samples by comparing the densities of the non-reinforced and reinforced samples. The increase in relative density can be explained by its high electrical and thermal conductivity, and the thermal conductivity of graphene may have improved the heat distribution during sintering by increasing its sintering performance [36-38]. For the Al6061-20$Al_2O_3$-yFLG samples, the FLG reinforcement reduced the densification ratios compared to the non-reinforced Al20$Al_2O_3$ except for the 3 wt.% FLG addition. The reason for the decrease in relative density can be said to be the high amount of FLG aggregated at the Al grain boundaries [39]. In previous studies, researchers reported that increasing the amount of reinforcement raised the densification rates of the samples. Wang et al. produced graphene reinforced $Al_2O_3$-WC matrix ceramic composites. They found that the graphene reinforced sample has a higher relative density compared to the non-reinforced sample [38]. Akçamlı et al. prepared $B_4C$ reinforced Al matrix composites, and they observed that increasing the amount of $B_4C$ improved the relative density [40]. Yazdani et al. produced graphene and carbon nanotube reinforced $Al_2O_3$ composites. They reported that the lowest relative density was seen in the unreinforced samples, and the densification rates rose with increasing reinforcement [41].

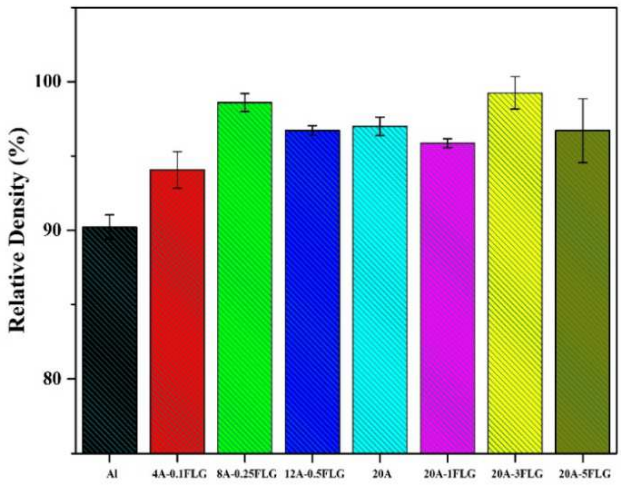


Fig. 3. Relative density values of sintered Al6061-x$Al_2O_3$-yFLG

The microstructures of the Al6061-x$Al_2O_3$-yFLG composites were investigated by LM and the micrographs are presented in Figures 4a-h. The LM micrographs show uniform distribution of $Al_2O_3$ and FLG throughout the matrix. What is more, highly densified structures with limited porosity can be seen in the overall microstructure of composites, and these results are compatible with the density results.

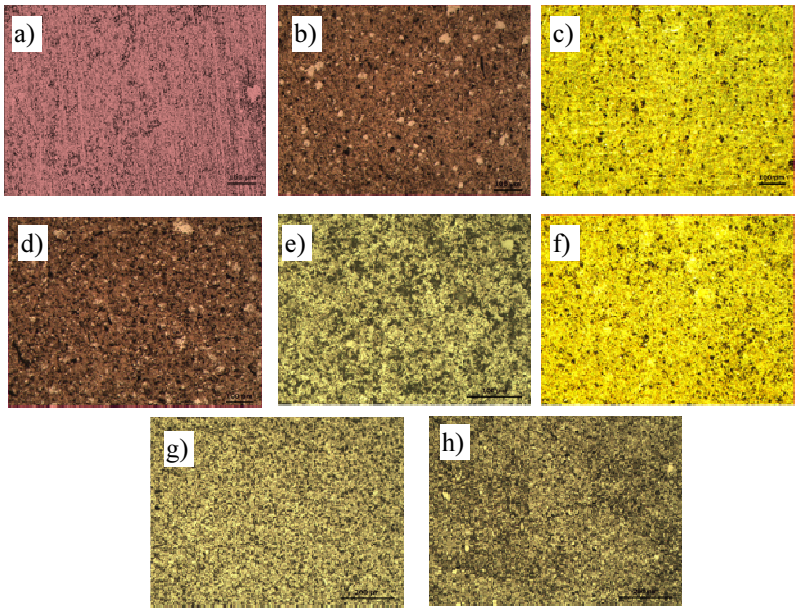


Fig. 4. LM micrographs of Al6061-x$Al_2O_3$-yFLG composites, a) Al, b) Al-4$Al_2O_3$-0.1FLG, c) Al-8$Al_2O_3$-0.25FLG, d) Al-12$Al_2O_3$-0.5FLG, e) Al-20$Al_2O_3$, f) Al-20$Al_2O_3$-1FLG, g) Al-20$Al_2O_3$-3FLG, h) Al-20$Al_2O_3$-5FLG

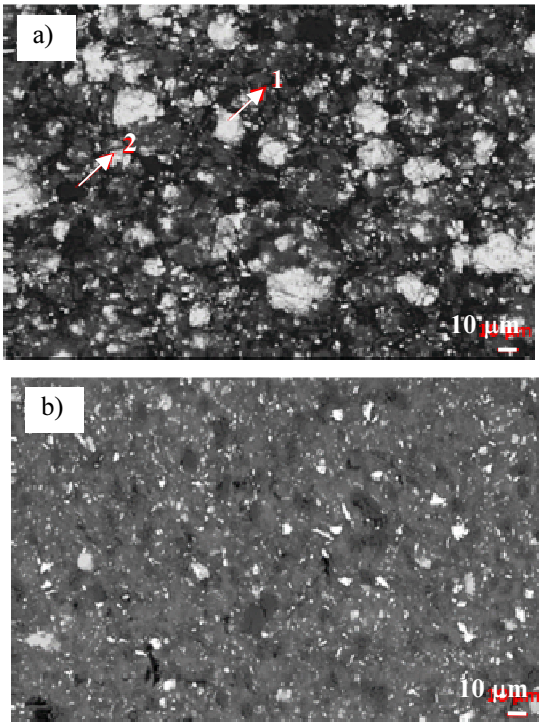


Fig. 5. SEM micrographs of Al6061-20$Al_2O_3$-1FLG composites

The SEM micrographs of the Al6061-x$Al_2O_3$-yFLG composites are shown in Figure 5. Moreover, the SEM micrographs and EDS mapping results for elements Al, C and O belonging to the Al6061-20$Al_2O_3$-1FLG composites are given in Figures 6a-e.

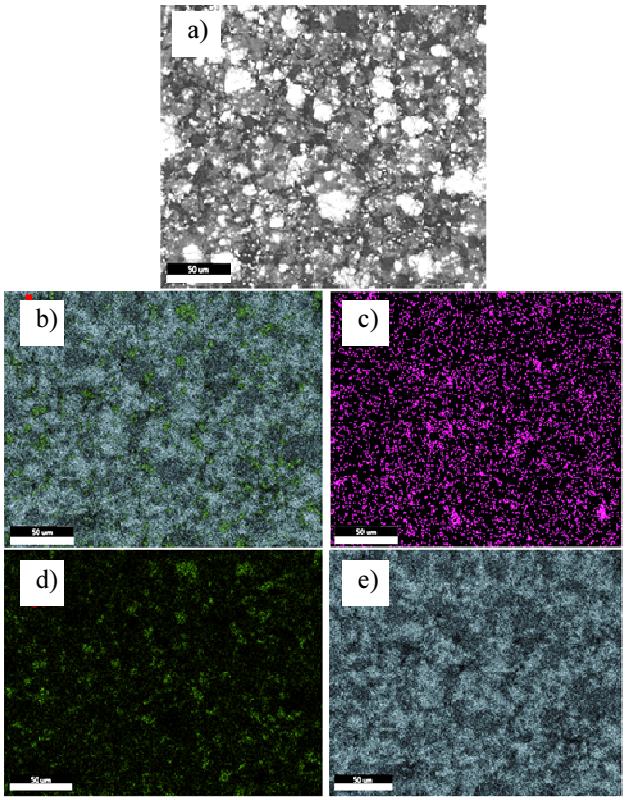


Fig. 6. a) SEM micrographs of Al6061-20$Al_2O_3$-1FLG sample and elemental mapping micrographs for (b) their overlapping mapping microcraphs, (c) C, (d) O, and (e) Al

Additionally, the results of the EDX compositional analyses of the marked phases in Figure 6 are given in Table 3. The SEM micrographs show that the structure consists of a matrix phase, bright white particles and dark regions. The EDX and mapping analysis results determined that the bright white particles in the structure are $Al_2O_3$, and the dark areas are the regions where the FLG particles are concentrated. Furthermore, as shown in Figure 6c, FLG exhibited homogenous distribution throughout the composite structure. Fe occurred due to the erosion of the steel grinding medium during MA. The results are consistent with previous literature studies [42-44].

TABLE 3. **EDX analyses results of regions numbered as 1, 2 in Figure 5**

| Marked regions in Figure 7 | Amounts of elements detected by EDX [wt.%] | | | |
|---|---|---|---|---|
| | Al | O | C | Fe |
| 1 | 64.6 | 20.9 | 8 | 6.5 |
| 2 | 64.1 | 31.7 | - | 4.2 |

The hardness values of the Al6061-x$Al_2O_3$-yFLG composites are given in Figure 7. The hardness values of the samples were found to be between 44.33 and 87.28 HV. There was a significant increase in the hardness of the reinforced samples compared to the samples without any reinforcement. The lowest hardness values were observed in the Al6061 sample – 44.33 HV. The highest hardness value was obtained by Al6061-20$Al_2O_3$-1FLG (87.28 HV) and the hardness increased twofold compared to Al6061. In addition, 1 wt.% FLG reinforcement increased the hardness by 54% compared to the non-FLG reinforced Al6061-20$Al_2O_3$ samples. Furthermore, increasing the FLG reinforcement from 1 to 3 and 5 wt.% caused a decrease in hardness from 87.28 to 67.71 and 65.98 HV, respectively.

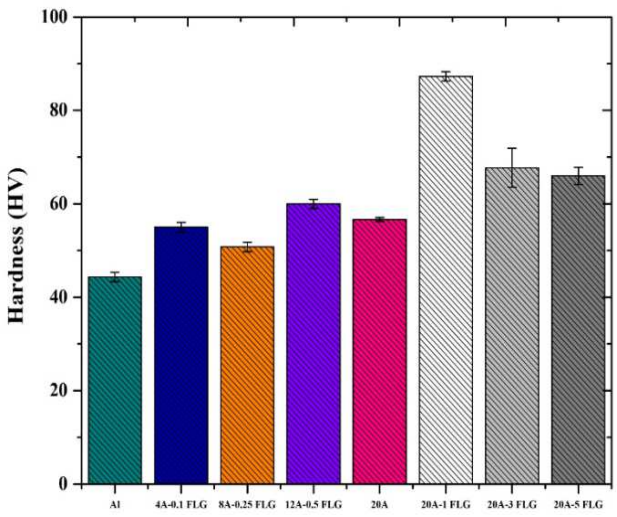


Fig. 7. Hardness values of Al6061-x$Al_2O_3$-xFLG (x = 0, 0.25, 0.50, 3 and 5 wt.%) composites

 

Similar results were obtained in previous studies in the literature. Şenel et al. [2] prepared $Al_2O_3$ and graphene reinforced Al matrix composites and investigated the mechanical properties of the composites. The highest hardness was found in the Al-30$Al_2O_3$ sample. The hardness properties were investigated by adding 0.1, 0.3 and 0.5 wt.% graphene to Al-30$Al_2O_3$. The highest hardness was detected in the 0.1 wt.% graphene reinforced composite. Additionally, the hardness decreased with an increasing amount of graphene. They suggested that the reason for this decrease in hardness was the clustering of graphene during the pressing process. Gao et al. [18] prepared Al-graphene composites by electrostatic self-assembly and the PM route. They found that the 0.3 wt.% graphene reinforced Al composites had the highest hardness and the lowest weight loss. However, it was found that increasing the graphene reinforcement from 0.3 to 0.5 wt.% caused a decrease in the hardness and wear resistance.

## CONCLUSIONS

In the present study, Al6061 matrix composites were prepared via MA, uniaxial pressing and pressureless sintering. The mechanical properties such as density, microstructure and hardness were investigated. The conclusions are as follows:

1. According to the XRD results, only α-Al and α-$Al_2O_3$ phases were observed for all the MAed powders and sintered samples. Furthermore, the peak related FLG was not found in the MAed powders or sintered samples. For the sintered samples, the XRD results show that $Al_4C_3$ was not formed in the structure.
2. The densification rates increased with reinforcement compared to the non-reinforced samples. The increase in relative density can be explained by the high electrical and thermal conductivity of graphene. Graphene may have improved the heat distribution during sintering, increasing the sintering performance. The highest relative density was detected for the Al6061-20$Al_2O_3$-3GNP composites.
3. The SEM micrographs, EDX and mapping results show that the microstructure of the composites consists of the matrix phase (Al6061), bright white particles ($Al_2O_3$) and dark regions (FLG). In addition, FLG exhibited homogenous distribution throughout the composite structure.
4. The analysis of the experimental results revealed a significant increase in the hardness of the AMC with reinforcement compared with the Al base alloy without reinforcement. The highest hardness values were observed as 87.28 HV for the Al6061-20$Al_2O_3$-1GNP composite, which was increased twofold compared to the Al6061. The optimum amount of FLG was found to be 1 wt.%, and a decrease in hardness occurred due to FLG agglomeration in the composites with greater amounts of this reinforcement.

The produced Al alloy possessing high relative density and hardness is a candidate for use in the automotive and aerospace industries. More detailed characterization studies are planned in future studies.

## REFERENCES


[1] Bastwros M., Kim G.-Y., Zhu C., Zhang K., Wang S., Tang X. et al., Effect of ball milling on graphene reinforced Al6061 composite fabricated by semi-solid sintering, Composites Part B: Engineering 2014, 60, 111-8.

[2] Can Şenel M., Gürbüz M., Investigation on mechanical properties and microstructures of aluminum hybrid composites reinforced with $Al_2O_3$/GNPs binary particles, Archives of Metallurgy and Materials 2021, 97-106-97.

[3] Cabeza M., Feijoo I., Merino P., Pena G., Pérez M., Cruz S. et al., Effect of high energy ball milling on the morphology, microstructure and properties of nano-sized TiC particle-reinforced 6005A aluminium alloy matrix composite, Powder Technology 2017, 321, 31-43.

[4] Akçamlı N., Küçükelyas B., Kaykılarlı C., Uzunsoy D., Investigation of microstructural, mechanical and corrosion properties of graphene nanoplatelets reinforced Al matrix composites, Materials Research Express 2019, 6(11), 115627.

[5] Avedesian M.M., Baker H., ASM Specialty Handbook: Magnesium and Magnesium Alloys: ASM International, 1999.

[6] Kumar G.V., Rao C., Selvaraj N., Studies on mechanical and dry sliding wear of Al6061-SiC composites, Composites Part B: Engineering 2012, 43(3), 1185-1191.

[7] Matli P.R., Fareeha U., Shakoor R.A., Mohamed A.M.A., A comparative study of structural and mechanical properties of Al-Cu composites prepared by vacuum and microwave sintering techniques, Journal of Materials Research and Technology, 2018, 7(2), 165-72.

[8] Abramovich H., Stability and Vibrations of Thin-walled Composite Structures, Woodhead Publishing 2017.

[9] Sivakumar S., Thimmappa S.K., Golla B.R., Corrosion behavior of extremely hard Al-Cu/Mg-SiC light metal alloy composites. Journal of Alloys and Compounds 2018, 767, 703-711.

[10] Koczak M.J., Khatri S.C., Allison J.E., Bader M.G., Metal-matrix Composites for Ground Vehicle, Aerospace, and industrial Applications, Butterworth-Heinemann 1993.

[11] Mohapatra J., Nayak S., Mahapatra M.M., Mechanical and tribology properties of Al-4.5% Cu-5% TiC metal matrix composites for light-weight structures, International Journal of Lightweight Materials and Manufacture 2020, 3(2), 120-126.

[12] Raju P.V.K., Rajesh S., Rao J.B., Bhargava N., Tribological behavior of Al-Cu alloys and innovative Al-Cu metal matrix composite fabricated using stir-casting technique, Materials Today: Proceedings 2018, 5(1), 885-896.

[13] Gireesh C.H., Prasad K.D., Ramji K., Vinay P., Mechanical characterization of aluminium metal matrix composite reinforced with aloe vera powder, Materials Today: Proceedings 2018, 5(2), 3289-97.

[14] Ramesh C., Khan A.A., Ravikumar N., Savanprabhu P., Prediction of wear coefficient of Al6061-$TiO_2$ composites, Wear 2005, 259(1-6), 602-608.

[15] Kumar G.V., Rao C., Selvaraj N., Bhagyashekar M., Studies on Al6061-SiC and Al7075-$Al_2O_3$ metal matrix composites, Journal of Minerals & Materials Characterization & Engineering. 2010, 9(1), 43-55.


 

[16] Ezatpour H.R., Sajjadi S.A., Sabzevar M.H., Huang Y., Investigation of microstructure and mechanical properties of Al6061-nanocomposite fabricated by stir casting, Materials & Design 2014, 55, 921-928.

[17] Zamani S., Won J.S., Salim M., AlAmer M., Chang C.-W., Kumar P. et al., Ultralight graphene/graphite hybrid fibers via entirely water-based processes and their application to density-controlled, high performance composites, Carbon 2021, 173, 880-890.

[18] Gao X., Yue H., Guo E., Zhang S., Wang B., Guan E. et al., Preparation and tribological properties of homogeneously dispersed graphene-reinforced aluminium matrix composites, Materials Science and Technology 2018, 34(11), 1316--1322.

[19] Yang W., Zhao Q., Xin L., Qiao J., Zou J., Shao P. et al., Microstructure and mechanical properties of graphene nanoplates reinforced pure Al matrix composites prepared by pressure infiltration method, Journal of Alloys and Compounds 2018, 732, 748-758.

[20] Cotul U., Parmak E., Kaykilarli C., Saray O., Colak O., Uzunsoy D., Development of high purity, few-layer graphene synthesis by electric arc discharge technique, Acta Physica Polonica A. 2018, 134, 289-291.

[21] Asgharzadeh H., Sedigh M., Synthesis and mechanical properties of Al matrix composites reinforced with few-layer graphene and graphene oxide, Journal of Alloys and Compounds 2017, 728, 47-62.

[22] Daha M., Nassef B.G., Nassef M., Mechanical and tribological characterization of a novel hybrid aluminum/$Al_2O_3$/RGO composite synthesized using powder metallurgy, Journal of Materials Engineering and Performance 2021, 1-9.

[23] Omrani E., Moghadam A.D., Kasar A.K., Rohatgi P., Menezes P.L., Tribological performance of Graphite nanoplatelets reinforced Al and Al/$Al_2O_3$ self-lubricating composites, Materials 2021, 14(5), 1183.

[24] Kumar H.P., Xavior M.A., Fatigue and wear behavior of Al6061-graphene composites synthesized by powder metallurgy, Transactions of the Indian Institute of Metals 2016, 69(2), 415-419.

[25] Pournaderi S., Akhlaghi F., Wear behaviour of Al6061-$Al_2O_3$ composites produced by in-situ powder metallurgy (IPM), Powder Technology 2017, 313, 184-190.

[26] Mercado-Lemus V.H., Gomez-Esparza C.D., Díaz-Guillén J.C., Mayén-Chaires J., Gallegos-Melgar A., Arcos-Gutierrez H. et al., Wear dry behavior of the Al-6061-$Al_2O_3$ composite synthesized by mechanical alloying, Metals 2021, 11(10), 1652.

[27] Boppana S.B., Dayanand S., Murthy B.V., Nagaral M, Telagu A., Kumar V. et al., Development and mechanical characterisation of Al6061-Al2O3-graphene hybrid metal matrix composites, Journal of Composites Science 2021, 5(6), 155.

[28] Soni S.K., Ganatra D., Mendiratta P., Reddy C., Thomas B., Microstructure and mechanical characterization of $Al_2O_3$/graphene reinforced Al6061 based hybrid nanocomposites, Metals and Materials International 2022, 28(2), 545-555.

[29] Kaftelen H., Ünlü N., Göller G., Öveçoğlu M.L., Henein H., Comparative processing-structure-property studies of Al-Cu matrix composites reinforced with TiC particulates, Composites Part A: Applied Science and Manufacturing 2011, 42(7), 812-824.

[30] Balaraj V., Kori N., Nagaral M., Auradi V., Microstructural evolution and mechanical characterization of micro $Al_2O_3$ particles reinforced Al6061 alloy metal composites, Materials Today: Proceedings 2021.

[31] Al-Mosawi B., Wexler D., Calka A., Characterization and mechanical properties of α-$Al_2O_3$ particle reinforced aluminium matrix composites, synthesized via uniball magneto-milling and uniaxial hot pressing, Advanced Powder Technology 2017, 28(3), 1054-1064.

[32] Prakash T., Sivasankaran S., Sasikumar P., Mechanical and tribological behaviour of friction-stir-processed Al 6061 aluminium sheet metal reinforced with $${{\rm Al} _ {2}{\rm O} _ {3}/0.5\,{\rm Gr}} $$ $Al_2O_3$/0.5 Gr hybrid surface nanocomposite, Arabian Journal for Science and Engineering 2015, 40(2), 559-569.

[33] Bharath V., Nagaral M., Auradi V., Kori S., Preparation of 6061Al-$Al_2O_3$ MMC's by stir casting and evaluation of mechanical and wear properties, Procedia Materials Science 2014, 6, 1658-1667.

[34] Kaykılarlı C., Uzunsoy D., Parmak E.D.Ş., Fellah M.F., Çakır Ö.Ç., Boron and nitrogen doping in graphene: an experimental and density functional theory (DFT) study, Nano Express 2020, 1(1), 010027.

[35] Wu Y., Wang B., Ma Y., Huang Y., Li N., Zhang F. et al., Efficient and large-scale synthesis of few-layered graphene using an arc-discharge method and conductivity studies of the resulting films, Nano Research 2010, 3(9), 661-669.

[36] Sun J., Zhao J., Huang Z., Yan K., Chen F., Jian Y. et al., Preparation and properties of multilayer graphene reinforced binderless TiC nanocomposite cemented carbide through two-step sintering, Materials & Design 2020, 188, 108495.

[37] Nieto A., Lahiri D., Agarwal A., Graphene nanoplatelets reinforced tantalum carbide consolidated by spark plasma sintering, Materials Science and Engineering: A. 2013, 582, 338-346.

[38] Wang X., Zhao J., Cui E., Tian X., Sun Z., Effect of interfacial structure on mechanical properties of graphene reinforced $Al_2O_3$-WC matrix ceramic composite, Nanomaterials 2021, 11(6), 1374.

[39] Wang J., Guo L.-N., Lin W.-M., Chen J., Liu C.-L., Zhang S. et al., Effect of the graphene content on the microstructures and properties of graphene/aluminum composites, New Carbon Materials 2019, 34(3), 275-285.

[40] Akçamlı N., Şenyurt B., B4C particulate-reinforced Al-8.5 wt.% Si-3.5 wt.% Cu matrix composites: powder metallurgical fabrication, age hardening, and characterization, Ceramics International 2021, 47(5), 6813-6826.

[41] Yazdani B., Porwal H., Xia Y., Yan H., Reece M.J., Zhu Y., Role of synthesis method on microstructure and mechanical properties of graphene/carbon nanotube toughened $Al_2O_3$ nanocomposites, Ceramics International 2015, 41(8), 9813--9822.

[42] Mahmoud T.S., El-Kady E.-S.Y., Al-Shihiri A.S.M., Corrosion behaviour of Al/SiC and Al/$Al_2O_3$ nanocomposites, Materials Research 2012, 15(6), 903-910.

[43] Shanmughasundaram P., Investigation on the wear behaviour of eutectic Al-Si Alloy-$Al_2O_3$-graphite composites fabricated through squeeze casting, Materials Research 2014, 17(4), 940-946.

[44] Elshina L., Muradymov R., Kvashnichev A., Vichuzhanin D., Molchanova N., Pankratov A., Synthesis of new metal-matrix Al-$Al_2O_3$-graphene composite materials, Russian Metallurgy (Metally) 2017, 2017(8), 631-641.

 